ISSN 1070-3632, Russian Journal of General Chemistry, 2024, Vol. 94, No. 9, pp. 2321–2330. © Pleiades Publishing, Ltd., 2024.

CuO-Catalyzed Synthesis, Characterization, and Computational Studies of Ethyl 2-Cyano-3-(1*H*-indol-3-yl)-3-phenylpropanoate Derivatives

A. K. Mishra[a], R. Das[a,*], G. Serdaroğlu[b,], J. Pandit[c], P. Mishra[a], A. K. Bahe[a], and N. Shukla[d]**

[a] *Heterocyclic Synthesis and Electroanalytical Laboratory, Department of Chemistry, Dr. Harisingh Gour Central University, Sagar, 470003 India*
[b] *Sivas Cumhuriyet University, Department of Mathematics and Science Education, Sivas, 58140 Turkey*
[c] *School of Sciences, SDGI Global University, Ghaziabad, 201015 India*
[d] *Smart Materials Research Institute, Southern Federal University, Rostov-On-Don, 344090 Russia*
**e-mail: ratneshdas1@gmail.com; **e-mail: goncagul.serdaroglu@gmail.com*

Received April 20, 2024; revised August 9, 2024; accepted August 9, 2024

Abstract—A one-pot multicomponent method employing substituted indole, ethyl cyanoacetate and aromatic aldehyde was found as an effective catalytic procedure for the synthesis of a novel indole derivatives. The potential of CuO nanoparticles as nanocatalysts for the Knoevenagel condensation and the synthesis of new indole derivatives was investigated. X-Ray diffraction was used to measure the size of the CuO nanoparticles. CuO nanoparticles can be recycled and used again after the reaction course. The ADMET analysis and drug-likeness results indicated that indole derivatives satisfied Lipinski's principles and drug-likeness requirements. The reactivity indices and potential areas obtained from the FMO experiments were successfully used to a range of molecular systems because they yield valuable information. Here, we determined the oxobutanoate derivative's critical areas and likely reactivity directions. The resultant indole derivatives were subjected to various analytical techniques, including mass spectroscopy, ^{1}H and ^{13}C NMR spectroscopy, FT-IR and mass spectrometry.

Keywords: substituted indole, ethyl cyanoacetate, aromatic aldehyde, CuO nanoparticles, X-ray diffraction FMO

DOI: 10.1134/S1070363224090135

INTRODUCTION

Heterocyclic compounds are found in large quantities in nature. Numerous heterocyclic substances are essential to the biological systems of all living things, including plants and animals. Synthetic heterocyclic compounds are significant because of its wide and diverse range [1]. The five, six, or seven-membered heterocyclic rings that make up nitrogen, oxygen, and sulfur have attracted the attention of scientists over the decades of historical advancement in organic synthesis. Today several drugs are synthesized in a day, and now for designing novel drug scaffolds. It is important because it helps to sketch molecules with heterocycles [2]. The indole moiety serves as an example of a crucial favored structure that can be used to identify novel therapeutic compounds. It consists of a bicyclic structure in which the pyrrole ring merges in two out of three locations with a six-membered benzene ring [3]. It's a crucial structural component of a wide range of substances, including indigoids and alkaloids. Additionally, it is present in several biological substances, including serotonin, reserpine, tryptophan, sumatriptan, melatonin, indomethacin, and vinblastine [4]. Because of this, substances with an indole ring have a wide range of pharmacological uses, including those that are antioxidant [5], antiviral [6], antibacterial [7], antifungal [8], anti-inflammatory [9], antimalarial [10], antileishmanial [11], antioxidant and anticancer [12]. Given this, the development of atom-efficient and systematic processes for the synthesis of indoles from recently disclosed starting materials remains a compelling research topic.

The small size and high surface-to-volume ratio, which alters their chemical and physical properties when compared to bulk materials with similar chemical composition, nanostructure catalysts play a significant role

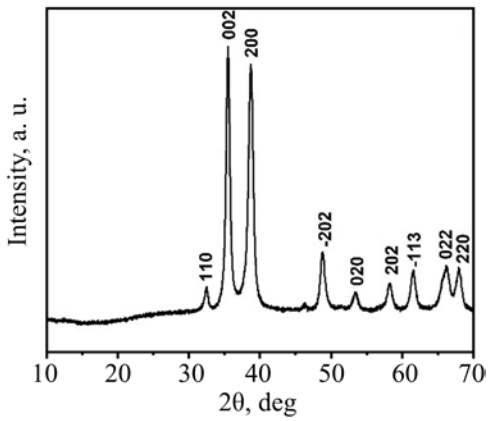

Fig. 1. XRD of CuO nanoparticles.

in the synthesis of organic materials [13]. The synthesis of a low-cost, non-toxic, and reusable nanocatalyst for organic reactions continues to be of interest to synthetic organic chemists. Metal oxide nanoparticles and their nanocomposite are synthesized for usage as a catalyst in organic synthesis [14]. The photocatalytic activity of CuO nanoparticles is well known. Redox reactions in particular may be fueled by light energy and occur at very low temperatures. This property makes them useful for environmental remediation processes including air purification and the breakdown of organic contaminants found in wastewater [15, 16]. The catalytic function of CuO is dependent on its essential geometric and electrical characteristics, indicating their combined importance in promoting catalysis [17]. In the recent decade, CuO nanocatalysts used in various organic synthesis, synthesis of *N*-arylation of indoles and amines derivatives [18, 19], and synthesis of 3-alkylated indole derivatives [20]. This study focused on synthesis of ethyl 2-cyano-3-(1*H*-indol-3-yl)-3-phenyl propanoate derivatives, novel compounds with potential antimicrobial properties. The CuO nanocatalyst required for the synthesis was produced through the sol-gel method [21]. A considerable effort has been made for the synthesis of ethyl 2-cyano-3-(1*H*-indol-3-yl)-3-phenylpropanoate derivatives due to their wide applications.

RESULTS AND DISCUSSION

Characterization of CuO nanoparticles. The X-ray diffraction of CuO nanoparticles was carried out to determine structural properties (Fig. 1). The pattern shows peaks at 32.54° (110), 35.45° (002), 38.71° (200), 48.93° (–202), 53.37° (020), 58.16° (020), 61.47° (–113), 66.26° (022) and 68.10° (220). The peaks were aligned using JCPDS software and it was matched well with the copper oxide (CuO). The crystallite size (*D*) was calculated for maximum intensity peak at 2θ = 43.20° (200) plane, by using the Debye–Scherrer equation:

$$D = \frac{k\lambda}{\beta \cos\theta}, \quad (1)$$

where *D* (nm) is crystallite size, *k* is a constant (0.94), λ (CuK_α = 1.54 Å) is the wavelength of the X-ray radiation, β is full width at half maximum for most intense peaks, and θ is Bragg's angle. The crystallite size for the (002) plane was 12.03 nm.

The FESEM was performed (Fig. S1, see Supplementary Information) for analysis of the surface morphology of anatase CuO nanoparticles. SEM image of CuO nanoparticle shows agglomerated spherical shape particles. In addition, EDX analysis of CuO nanoparticles was carried out, which exhibits the elemental composition peaks of Cu (56.72%) and O (43.28%) in the prepared anatase CuO nanoparticles.

Chemistry. In this work, aromatic aldehyde, ethyl cyanoacetate, and substituted indole substrates were reacted in ethanol as a solvent for two to three hours in the presence of a heterogeneous catalyst (CuO), to synthesize propanoate derivatives **4a**–**4j** (Scheme 1, Table S1, see Supplementary Information). By creating a more reactive intermediate, copper oxide can catalyze the model reaction and expedite the multi-component process. In this instance, the reaction starts with the active methylene group attacking the aromatic aldehyde group's carbon atom. This is followed by Knoevenagel condensation, which eliminates the water molecule. Consequently, substantial yields were obtained when CuO was employed as a dehydrating agent and to accelerate the last stage of the Michael addition reaction. Overall, the reactions went smoothly and produced substantial volumes. An ester group in a molecule can be positively identified using the strong infrared absorption band in the 1735–1727 cm^{-1} region, which is linked to the stretching vibration of the carbon-oxygen double bond. The molecular environment surrounding the ester group determines the band's location in this frequency range. The ester frequency varies from 1735 to 1727 cm^{-1} for each compound. In addition to the characteristic sharp bands caused by N–O stretching at 1447–1500 cm^{-1}, the

Scheme 1.

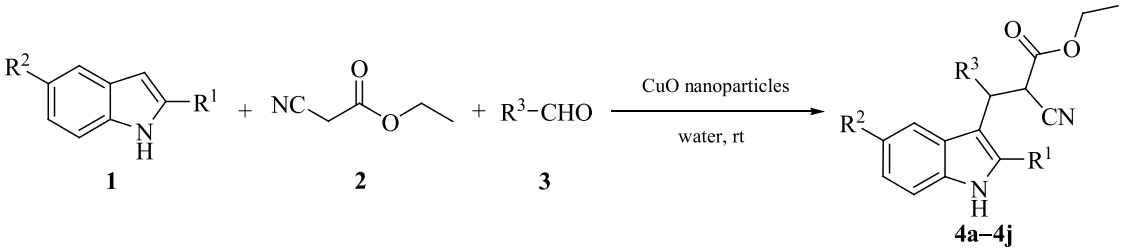

R^1 = H, R^2 = H, R^3 = Ph (**a**); R^1 = Ph, R^2 = H, R^3 = 4-NO_2Ph (**b**); R^1 = Me, R^2 = H, R^3 = 3-NO_2Ph (**c**); R^1 = Ph, R^2 = H, R^3 = thiophen-2-yl (**d**); R^1 = Me, R^2 = H, R^3 = 2,4-diClPh (**e**); R^1 = Me, R^2 = H, R^3 = 2-MePh (**f**); R^1 = Me, R^2 = H, R^3 = 2-ClPh (**g**); R^1 = H, R^2 = Br, R^3 = 4-NO_2Ph (**h**); R^1 = H, R^2 = Br, R^3 = 3-NO_2Ph (**i**); R^1 = H, R^2 = Br, R^3 = 2,4-diClPh (**j**).

C–Cl group in the molecule also causes some stretching frequency at 750–735 cm^{-1}. Several compounds show well-defined, strong stretching bands at 650–600 cm^{-1} for C–Br groups. Every molecule has a base peak and a molecular ion peak in mass spectra. The existence of daughter ions in the mass spectra is indicated by fragmentation patterns that correspond with pertinent compound research.

The compounds under investigation's ^{1}H NMR spectra in $CDCl_3$ showed distinct signals at various places. Doublets are seen at 4.88–4.34, 4.90–4.34, 4.84–8.29, 4.85–4.33, and 4.88–4.25 ppm for compounds **4a**, **4b**, **4c**, **4d**, and **4e**, respectively. A quartet is seen at 3.96 ppm and a triplet at 1.07 ppm in compound **4a**. Every peak of the benzene ring is found in the aromatic zone, which is found at around 7 ppm. The carbonyl carbon of the ester displays signals at 168.0 ppm in the ^{13}C NMR spectra, whereas the $COCH_3$ group is detected in the downfield region at 202.9 ppm. Furthermore, for compound **4a**, the OCH_2 group is detected at 61.5 ppm, while the CH_3 group is detected at 13.7 ppm.

Table 1. The optimization of solvents in the reaction of indole **1** with benzaldehyde **3** catalyzed by CuO nanocatalyst

Entry	Solvent	Time, h	Yield, %[a]
1	Ethanol	3	82
2	Toluene	9	43
3	Methanol	16	62
4	Water	3	73
5	CH_3CN	3.5	74

[a] Yields referred to the isolated yield.

To improve the reaction conditions, the impact of several solvents was also investigated (Table 1), and it was found that ethanol was an efficient solvent. The solvent for the reaction involving substituted indole, ethyl cyanoacetate, and aromatic aldehyde in the presence of CuO nanocatalysts was carefully optimized at room temperature using a variety of solvents. The best solvent, ethanol, was shown to shorten the reaction time and increase the yield of product **4**. On the other hand, polar solvents like water and MeOH decrease the solubility of the reactant, which reduces the reactivity.

Additionally, we examined how many CuO nanocatalysts would be the best to use in this reaction on 1 mmol scale. The addition of 25 mg of CuO nanoparticles improved the process under the same conditions, but did not increase the yield. In 76% and 82% yield of the reactions, the final product was produced when the dosage of CuO nanocatalysts was increased from 15 to 20 mg. Therefore, the best outcomes were obtained with 20 mg of CuO nanocatalysts. The addition of more catalysts did not significantly improve the results.

The effect of varying amounts of CuO nanocatalysts on the yield of the reaction was systematically studied. There was a 60% yield from the reaction when 15 mg of the catalyst was applied. The yield increased to 80% when the catalyst dosage was increased to 20 mg. However, further increasing the catalyst amount to 25 mg did not result in any additional increase in yield, which remained at 80%. Therefore, the optimal catalyst loading was determined to be 20 mg, which provided the highest yield without requiring excess catalyst. The reaction efficiency did not significantly increase with the addition of additional catalysts after this stage.

Scheme 2.

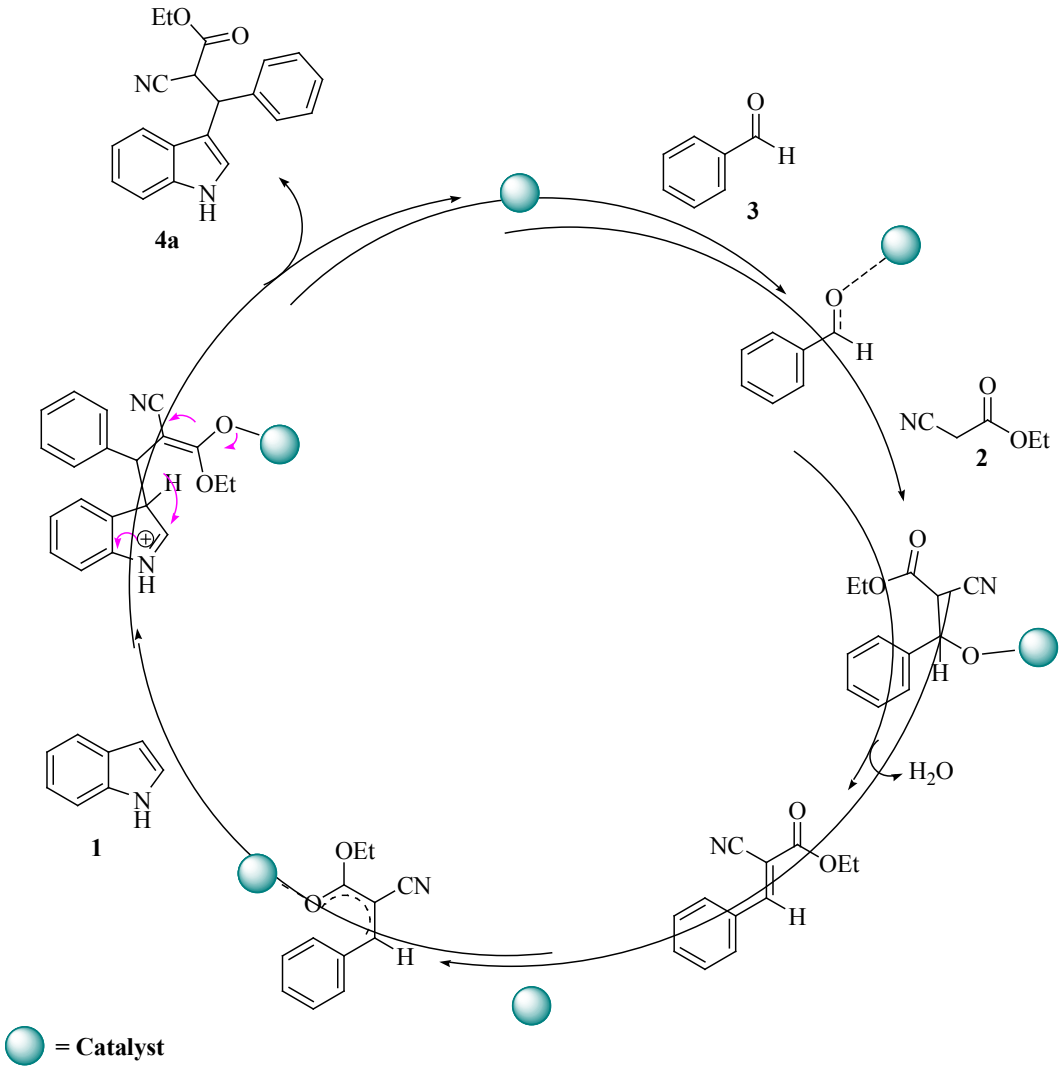

In the mechanism (Scheme 2), aldehyde reacts with ethyl cyanoacetate, in the presence of CuO nanoparticles, which act as a catalyst to activate the substrate molecules, leading to the formation of the Knoevenagel adduct. The indole derivative then undergoes a Michael addition to the double bond of the Knoevenagel adduct and a series of proton transfers occur, leading to the final product.

DFT computational study. All DFT computations of the studied indoles **4a**–**4j** were conducted by G09W [22] software, with B3LYP/6-311G** [23–26] level and using default scheme [27, 28]. The illustration of the optimized structures and HOMO and LUMO and MEP plots were done by the GaussView 6.0.16 [29] package. In all computations, the optimized and confirmed structures with a lack of the imaginary frequency were used.

The reactivity indexes of the compounds were calculated by using the ionization energy I and electron affinity A [30], which can be obtained from the frontier molecular orbital energies.

$$I = -E_{\mathrm{HOMO}}, \tag{2}$$

$$A = -E_{\mathrm{LUMO}}. \tag{3}$$

The definition of the reactivity indexes as follows: χ is electronic chemical potential, η is global hardness, ω is electrophilicity, $\Delta N_{\max}$ is the maximum charge transfer capability index [31–36], ω^- is the electrodonating power

Table 2. The physicochemical values at B3LYP/6-311G** level

Compound	ΔE, Hartree	ΔH, Hartree	ΔG, Hartree	$\Delta E_{ther.}$, kcal/mol	C_v, cal mol^{-1} K^{-1}	S, cal mol^{-1} K^{-1}	DM, D	α, a. u.
4a	–1032.829489	–1032.807289	–1032.882557	223.743	80.393	158.415	7.059	222.238
4b	–1468.409696	–1468.380036	–1468.474201	280.392	108.281	198.187	8.553	311.726
4c	–1276.684527	–1276.657948	–1276.743677	245.152	95.043	180.432	5.323	250.803
4d	–1584.657320	–1584.630436	–1584.718474	256.147	97.659	185.290	4.476	289.025
4e	–1991.384875	–1991.358419	–1991.443284	231.517	94.135	178.613	5.912	261.285
4f	–1111.430113	–1111.404489	–1111.487521	260.583	92.358	174.756	4.987	248.558
4g	–1531.755086	–1531.729925	–1531.811246	236.796	90.259	171.156	5.450	246.702
4h	–3810.932866	–3810.906486	–3810.993523	221.377	93.339	183.185	8.331	258.470
4i	–3810.934459	–3810.908163	–3810.994377	221.397	93.308	181.453	4.504	255.717
4j	–4525.635196	–4525.609017	–4525.694421	207.756	92.402	179.748	5.553	265.994

and ω^+ is the electroaccepting power [37], and $\Delta E_{back\text{-}donat}$ is back-donation energy [38].

Lipophilicity and water solubility study. The lipophilic characters of the indole derivatives were calculated according to the approaches as follows: ILOGP [39], XLOGP3 [40], WLOGP [41], MLOGP [42], and SILICOS-IT [43] using the SwissADME [44] tools. log *P* index is given by the following formula:

$$\log P_{o/w} = \log \frac{c_o}{c_w}. \quad (4)$$

In addition, the water-soluble behaviors of the indoles were also calculated according to three approaches such as Delaney [45] and Ali [46], and the fragmental [43] approach.

The possible drug-likeness features of the indoles were determined by using the methods as follows: Lipinski's [42], Ghose [47], Veber [48], Egan [49], and Muegge [50] rules; and the Abbott score [51] was used to predict the bioavailability scale.

Molecule geometries and thermochemistry. As known well, the thermochemical properties of molecular systems play a great role in the elucidation/prediction of the physicochemical processes. In this respect, the calculated thermochemical and physical values of the optimized (Fig. S2, see Supplementary Information) **4a**–**4j** compounds were given in Table 2.

From Table S2 (see Supplementary Information), the thermochemical functions ΔE, ΔH, and ΔG of the compound **4a** were calculated in –1032.829489, –1032.807289, and –1032.882557 a. u., respectively. Moreover, the ΔE_{ther}, C_v, and S values of **4a** were predicted in 223.743 kcal/mol, 80.393, and 158.415 cal mol^{-1} K^{-1}, respectively, which were the lowest values among the investigated molecules as expected. Namely, the **4a** molecule has 42 atoms and thus has 120 freedom degrees, whereas the **4b** has 54 atoms and thus 156 freedom degrees. Thus, the ΔE_{ther}, C_v, and S values of **4b** were estimated at 280.392 kcal/mol, 108.281, and 198.187 cal mol^{-1} K^{-1}, respectively, which were the highest ones. Moreover, the highest DM and α values among the compounds were predicted for **4b** in 8.553 D and 311.726 a. u., respectively. From Table 2, the smallest dipole moment among the compounds was determined for the **4d** molecule including the thiophene substitution at 4.476 D. On the other hand, the **4j** molecule has also 42 atoms, but it includes the Cl and Br atoms substituted on the phenyl ring instead of the H of **4a**; ΔE_{ther}, C_v, and S values of **4j** were found to be in 207.756 kcal/mol, 92.402, and 179.748 cal mol^{-1} K^{-1} respectively. Also, the ΔE, ΔH, and ΔG of the compound **4j** were computed in –4525.635196, –4525.609017, and –4525.694421 a. u. which were the greatest values as expected from molecular topology and quantum statistics [52–54] because of the presence of the Br and Cl substitutions. On the other hand, the NO_2 group position on **4h** and **4i** compounds affected the dipole moments of them mostly, and slightly the polarizability. Namely, the DM and α values of the **4h** molecule, which included the NO_2 group on *para*-position, were determined at 8.331 D and 258.470 a. u., respectively. However, these values of **4i** which included the NO_2 group on *meta*-position, were found to be at 4.504 D and 255.717 a. u., respectively.

Table 3. Drug-likeness scores

Compound	Lipinski	Ghose	Veber	Egan	Muegge	Bioavailability
4a	Yes	Yes	Yes	Yes	Yes	0.55
4b	Yes	No; WLOGP > 5.6	Yes	No; WLOGP > 5.88	No; XLOGP3 > 5	0.55
4c	Yes	Yes	Yes	Yes	Yes	0.55
4d	Yes	No; WLOGP > 5.6	Yes	No; WLOGP > 5.88	No; XLOGP3 > 5	0.55
4e	Yes	No; WLOGP > 5.6	Yes	Yes	No; XLOGP3 > 5	0.55
4f	Yes	Yes	Yes	Yes	Yes	0.55
4g	Yes	Yes	Yes	Yes	Yes	0.55
4h	Yes	Yes	Yes	Yes	Yes	0.55
4i	Yes	Yes	Yes	Yes	Yes	0.55
4j	Yes	No; WLOGP > 5.6	Yes	No; WLOGP > 5.88	No; XLOGP3 > 5	0.55

Lipophilicity and water solubility. In addition to the thermochemical properties, the lipophilic and water solubility characteristics of the compounds were calculated and presented in Table S2 (see Supplementary Information).

Accordingly, ILOGP approach disclosed the lipophilicity order of **4a**–**4j**. On the other hand, the MLOGP method exhibited the log $P_{o/w}$ order of **4a**–**4j**. The other approaches revealed the following orders for the lipophilicity of the compounds.

From all results, the lipophilicity index seems to depend on the approach used. But still, the **4d** with the thiophene substitution would present more lipophilic character than the others, whereas the **4c** would exhibit less lipophilic among the compounds according to the averaged log $P_{o/w}$. Based on the WLOGP and XLOGP3 approaches, the **4a** compound would be less lipophilic.

According to the ESOL method, all compounds could be moderately soluble in the water, except for **4d** and **4j** which were determined as poorly soluble. Namely, the log *S* (ESOL) order of the compound was found to be **4a**–**4j**. On the other hand, the log *S* (Ali) method presented the order of **4a**–**4j**; **4a** and **4f** would be moderately soluble while the others would present poorly soluble properties in the water. Moreover, all compounds were poorly soluble depending on the log *S* (SILICOS-IT) results. Still, it could be said that the Ph, NO_2, and halogen substitution may affect the decrease in the water solubility since the most soluble compound was determined as the **4a** structure.

In addition, the drug-likeness and then bioavailability indexes of the compounds are presented in Table 3. According to the Lipinski and Veber rules, all compounds could be suitable structures in terms of drug-likeness. On the other hand, **4b**, **4d**, **4e**, and **4j** would not be promising due to the WLOGP > 5.6 violation depending on the Ghose rules. Similarly, the XLOGP3 score based on the Muegge approach was predicted higher than 5 which means that **4b**, **4d**, **4e**, and **4j** compounds could not be proper agents in terms of drug likeness. According to the Egan approach, **4b**, **4d**, and **4j** molecules would have WLOGP > 5.88 violation, but the other molecules could be suitable. Fortunately, the bioavailability indexes of all compounds were predicted 0.55, remarkable.

FMOs and MEP studies. The possible reactivity tendency and regions of the molecular systems have placed an important role in evaluation and comparison purposes in contemporary studies [55–57]. Herein, the predicted reactivity indexes of the compound are presented in Table 4.

From the $\Delta E(L–H)$ results, the compound **4a** would rather prefer to interact to an outer molecular system than the intramolecular interactions, whereas the **4b** would like to prefer the intramolecular interactions. In addition, the **4i** (χ = –5.028 eV) could be more stable than the other compounds whereas the **4d** would be less stable (χ = –4.046 eV) one among the compounds, because of the electronic chemical potential orders of the compounds. Depending on the η (eV) order of the compounds, **4b** (2.066 eV) might be a softer compound while **4a** (2.763 eV) would be the hardest molecule among the studied compounds. The ω (eV) results indicate that the **4i** (0.218 eV) could present more electrophilic character whereas the **4f** (0.115 eV) would exhibit less electrophilic character. Furthermore, the **4i** would have the biggest electrodonating (ω^- = 0.320 a. u.) and electroaccepting (ω^+ = 0.135 a. u.) potency. Among the studied compounds,

Table 4. The chemical reactivity indexes at the B3LYP/6-311G** level

Parameter	**4a**	**4b**	**4c**	**4d**	**4e**	**4f**	**4g**	**4h**	**4i**	**4j**
H (–I), eV	–7.033	–6.890	–7.128	–6.589	–6.988	–6.821	–6.890	–7.223	–7.163	–7.034
L (–A), eV	–1.508	–2.758	–2.823	–1.503	–1.514	–1.414	–1.392	–2.808	–2.893	–1.829
ΔE (L–H), eV	5.525	4.132	4.305	5.086	5.474	5.407	5.498	4.415	4.271	5.205
χ, eV	–4.270	–4.824	–4.975	–4.046	–4.251	–4.117	–4.141	–5.015	–5.028	–4.432
η, eV	2.763	2.066	2.153	2.543	2.737	2.704	2.749	2.208	2.135	2.602
ω, eV	0.121	0.207	0.211	0.118	0.121	0.115	0.115	0.209	0.218	0.139
ω^+, a. u.	0.056	0.128	0.130	0.056	0.056	0.052	0.051	0.127	0.135	0.069
ω^-, a. u.	0.212	0.305	0.313	0.204	0.212	0.203	0.203	0.312	0.320	0.232
ΔN_{max}, eV	1.546	2.335	2.311	1.591	1.553	1.523	1.506	2.272	2.355	1.703
$\Delta E_{back\text{-}donat}$, eV	–0.691	–0.516	–0.538	–0.636	–0.684	–0.676	–0.687	–0.552	–0.534	–0.651

4i (ΔN_{max} = 2.355 eV) would have more electron transfer potency while **4g** (ΔN_{max} = 1.506 eV) would have less potency. From the obtained results, the CH_3 and Ph group substitutions on the indole part of the compounds caused the stabilization via back donation decrease. Also, NO_2, halogen(s), and CH_3 substitutions on the phenyl ring made the stabilization energy lowering via back donation.

For the **4a** molecule, the indole ring would have a critical role in both the electrophilic and nucleophilic attacks in addition to the benzylic ring for the electrophilic attacks, due to the electron localization on the molecular surface. Also, the HOMO density of the **4b** molecule appeared on the indole and benzylic ring, whereas the LUMO of this molecule localized on the *p*-NO_2-Ph ring as well as the indole ring. The HOMO of the **4c** compound was distributed on the *p*-NO_2-Ph ring while the LUMO separated on rings of the compound except for the cyanopropanoate chain. From Fig. S3 (see Supplementary Information), the HOMO density for **4e**, **4g**, and **4j** molecules only expanded on the indole rings, whereas the HOMO for **4d**, **4e**, **4g**, and **4j** compounds seem on the substituted ring except for the indole part. From Fig. S4 (see Supplementary materials), the LUMO of **4d** localized on the indole and bonded Ph group, whereas the LUMO of **4e** and **4j** densified on the indole part of the molecules. On the other hand, the LUMO of **4f** and **4g** could expand as half on the substituted ring as well as the indole ring. For all compounds, the red color as a marker of the electron abundance region would occur on the O and N atoms in the cyanopropanoate chain (Fig. S5, see Supplementary Information). Also, the blue color as a sign of the electron-poor region would appear on the CH_2 group of the indole ring. On the other hand, the remarkably blue color of the **4d** molecule would also appear close to the S atom of the thiophene ring. Moreover, the Ph ring for all compounds could be seen by yellow color as an indicator of the electron-rich region in a moderate level.

CONCLUSIONS

In this study, the synthesis of various ethyl 2-cyano-3-(1*H*-indol-3-yl)-3-phenyl propanoate derivatives was performed. Structure of the prepared compounds was confirmed through FT-IR, ^{1}H, ^{13}C NMR and MS spectroscopy methods. The synthesis of these indole derivatives was catalyzed by the synthesized CuO nanoparticles, which offer a larger surface area and act as highly efficient catalysts. The use of CuO nanoparticles not only shortened reaction times but also facilitated easier catalyst recovery compared to conventional synthesis methods. The catalyst was successfully removed from the reaction mixture and reused after a straightforward purification process, with its reusability demonstrated through a separation test using a separating funnel. This research highlights a sustainable and efficient approach to synthesizing biologically active compounds, combining green synthesis principles with the antimicrobial evaluation of novel ethyl 2-cyano-3-(1*H*-indol-3-yl)-3-phenyl propanoate derivatives.

AUTHOR INFORMATION

A.K. Mishra, ORCID: https://orcid.org/0000-0003-2862-3384

R. Das, ORCID: https://orcid.org/0000-0002-5575-8359

G. Serdaroğlu, ORCID: https://orcid.org/ 0000-0001-7649-9168

J. Pandit, ORCID: https://orcid.org/0000-0002-0024-1977

P. Mishra, ORCID: https://orcid.org/0000-0003-0927-2857

A.K. Bahe, ORCID: https://orcid.org/0000-0001-5733-1685

N. Shukla, ORCID: https://orcid.org/0000-0001-5379-5589

ACKNOWLEDGMENTS

Authors thanks the University Grant Commission (India) for the fellowship, and Sophisticated Instrumentation Centre, Dr. Hari Singh Gour Central University for all the necessary characterizations and lab facilities. Authors are also grateful to the Scientific and Technological Research Council of Turkey (TUBITAK). All quantum chemical calculations were Performed at the High Performance and Grid Computing Center (TR-Grid e-Infrastructure).

FUNDING

This work was supported by ongoing institutional funding. No additional grants to carry out or direct this particular research were obtained.

CONFLICT OF INTEREST

The authors declare no conflict of interest.

SUPPLEMENTARY INFORMATION

The online version contains supplementary material available at https://doi.org/10.1134/S1070363224090135.

REFERENCES

1. Alvarez-Builla, J., Vaquero, J.J., and Barluenga, J., *Modern Heterocycl. Chemistry*, Weinheim: Wiley-VCH, 2011, Vol. 4, p. 1989. https://doi.org/10.1002/9783527637737
2. Ebenezer, O., Jordaan, M.A., Carena, G., Bono, T., Shapi, M., and Tuszynski, J.A., *Int. J. Mol. Sci.,* 2022, vol. 23, p. 8117. https://doi.org/10.3390/ijms23158117
3. Jampilek, J., *Molecules,* 2019, vol. 24, p. 3839. https://doi.org/10.3390/molecules24213839
4. Heravi, M.M. and Zadsirjan, V., *RSC Adv.*, 2020, vol. 72, p. 44247. https://doi.org/10.1039/d0ra09198g
5. Jasiewicz, B., Kozanecka-Okupnik, W., Przygodzki, M., Warżajtis, B., Rychlewska, U., Pospieszny, T., and Mrówczyńska, L., *Sci. Rep.*, 2021, vol. 11, p. 1. https://doi.org/10.1038/s41598-021-94904-z
6. Dorababu, A., *RSC Med. Chem.*, 2020, vol. 11, p. 1335. https://doi.org/10.1039/d0md00288g
7. Song, F., Li, Z., Bian, Y., Huo, X., Fang, J., Shao, L., and Zhou, M., *Arch. Pharm.*, 2020, vol. 353, p. 1. https://doi.org/10.1002/ardp.202000143
8. Zheng, S., Jiang, Q., Massande, G.N., Wu, W., Lin, C., Fang, Y., Tan, Y., and Zhu, R., *Chem. Nat. Compd.,* 2023, vol. 59, p. 111. https://doi.org/10.1007/s10600-023-03929-5
9. Rudrapal, M., Celik, I., Chinnam, S., Çevik, U.A., Tallei, T.E., Nizam, A., Joy, F., Abdellattif, M.H., and Walode, S.G., *Polycycl. Arom. Compd.,* 2023, vol. 43, p. 7732. https://doi.org/10.1080/10406638.2022.2139733
10. Chauhan, M., Saxena, A., and Saha, B., *Eur. J. Med. Chem.,* 2021, vol. 218, p. 113400. https://doi.org/10.1016/j.ejmech.2021.113400
11. Sahu, N.K., Sharma, R., Suhas, K.P., Joshi, J., Prakash, K., Sharma, R., Pratap, R., Hu, X., Kaur, S., Jain, M., and Coluccini, C., *Molecules*, 2023, vol. 28, p. 4817. https://doi.org/10.3390/molecules28124817
12. Kaur, H., Singh, J., and Narasimhan, B., *BMC Chem.,* 2019, vol. 13, p. 1. https://doi.org/10.1186/s13065-019-0580-0
13. Kanagarajan, H., Gunabalan, M., Kajbafvala, A., Narayanan, A., Sompalle, R., and Roopan, S. M., *ChemInform*, 2014, vol. 45, p. 1. https://doi.org/10.1002/chin.201431259
14. Makawana, J.A., Sangani, C.B., Yao, Y.F., Duan, Y.T., Lv, P.C., and Zhu, H.L., *Mini-Rev. Med. Chem.,* 2016, vol. 16, p. 1303. https://doi.org/10.2174/1389557516666160823143243
15. Aroob, S., Carabineiro, S.A.C., Taj, M.B., Bibi, I., Raheel, A., Javed, T., Yahya, R., Alelwani, W., Verpoort, F., Kamwilaisak, K., Al-Farraj, S., and Sillanpää, M., *Catalysts,* 2023, vol. 13, p. 1. https://doi.org/10.3390/catal13030502
16. Naz, S., Gul, A., Zia, M., and Javed, R., *Appl. Microbiol. Biotechnol.*, 2023, vol. 107, p. 1039. https://doi.org/10.1007/s00253-023-12364-z
17. Dobrucka, R., *J. Inorg. Organomet. Polym. Mater.*, 2018, vol. 28, p. 812. https://doi.org/10.1007/s10904-017-0750-2
18. Nasrollahzadeh, M., Sajadi, S.M., Rostami-Vartooni, A., and Hussin, S.M., *J. Colloid Interface Sci.,* 2016, vol. 466, p. 113. https://doi.org/10.1016/j.jcis.2015.12.018

19. Khalil, A., Fihri, A., Jouiad, M., and Hashaikeh, R., *Tetrahedron Lett.,* 2014, vol. 55, p. 5973. https://doi.org/10.1016/j.tetlet.2014.08.120
20. Khan, G.A., War, J.A., Naikoo, G.A., Pandit, U.J., and Das, R., *J. Saudi Chem. Soc.,* 2018, vol. 22, p. 6. https://doi.org/10.1016/j.jscs.2016.03.009
21. Patel, M., Mishra, S., Verma, R., and Shikha, D., *Discov. Mater.*, 2022, vol. 2, p. 1. https://doi.org/10.1007/s43939-022-00022-6
22. Frisch, M.J., Trucks, G.W., Schlegel, H.B., Scuseria, G.E., Robb, M.A., Cheeseman, J.R., Scalmani, G., Barone, V., Mennucci, B., Petersson, G.A., Nakatsuji, H., Caricato, M., Li, X., Hratchian, H.P., Izmaylov, A.F., Bloino, J., Zheng, G., Sonnenberg, J.L., Hada, M., Ehara, M., Toyota, K., Fukuda, R., Hasegawa, J., Ishida, M., Nakajima, T., et al., Gaussian 09, Revision B.01. Gaussian Inc., Wallingford., Gaussian 09W, Revision D.01, Gaussian, Inc., Wallingford CT 2013.
23. Becke, A.D., *J. Chem. Phys*., 1993, vol. 98, p. 1372. https://doi.org/10.1063/1.464304
24. Lee, C., Yang, W., and Parr, R.G., *Phys. Rev. B*, 1988, vol. 37, p. 785. https://doi.org/10.1103/physrevb.37.785
25. Raghavachari, K., Binkley, J.S., Seeger, R., and Pople, J.A., *J. Chem. Phys*., 1980, vol. 72, p. 650. https://doi.org/10.1063/1.438955
26. McLean, A.D. and Chandler, G.S., *J. Chem. Phys*., 1980, vol. 72 p. 5639. https://doi.org/10.1063/1.438980
27. Li, X. and Frisch, M.J., *J. Chem. Theory Comput*., 2006, vol. 2, p. 835. https://doi.org/10.1021/ct050275a
28. Kudin, K.N., Scuseria, G.E., and Cancès, E., *J. Chem. Phys*., 2002, vol. 116, p. 8255. https://doi.org/10.1063/1.1470195
29. GaussView 6.0.16, Gaussian, Inc, Wallingford CT, 2016.
30. Koopmans, T., *Physica*, 1934, vol. 1, p. 104. https://doi.org/10.1016/s0031-8914(34)90011-2
31. Janak, J.F., *Phys. Rev. (B),* 1978, vol. 18, p. 7165. https://doi.org/10.1103/physrevb.18.7165
32. Perdew, J.P., Parr, R.G., Levy, M., and Balduz, J.L., *Phys. Rev. Lett.*, 1982, vol. 49, p. 1691. https://doi.org/10.1103/physrevlett.49.1691
33. Perdew, J.P. and Levy, M., *Phys. Rev. Lett.*, 1983, vol. 51, p. 1884. https://doi.org/10.1103/physrevlett.51.1884
34. Parr, R.G. and Pearson, R.G., *J. Am. Chem. Soc*., 1983, vol. 105, p. 7512. https://doi.org/10.1021/ja00364a005
35. Pearson, R.G., *Proc. Natl. Acad. Sci. USA*, 1986, vol. 83, p. 8440. https://doi.org/10.1073/pnas.83.22.8440
36. Parr, R.G., Szentpaly, L.V., and Liu, S., *J. Am. Chem. Soc*., 1999, vol. 121, p. 1922. https://doi.org/10.1021/ja983494x
37. Gazquez, J.L., Cedillo, A., and Vela, A., *J. Phys. Chem. (A)*, 2007, vol. 111, p. 1966. https://doi.org/10.1021/jp065459f
38. Gomez, B., Likhanova, N.V., Domínguez-Aguilar, M.A.,Martínez-Palou, R.,Vela, A., and Gazquez, J.L., *J. Phys. Chem. B,* 2006, vol. 110, p. 8928. https://doi.org/10.1021/jp057143y
39. Daina, A., Michielin, O., and Zoete, V., *J. Chem. Inf. Model*., 2014, vol. 54, p. 3284. https://doi.org/10.1021/ci500467k
40. Cheng, T., Zhao, Y., Li, X., Lin, F., Xu, Y., Zhang, X., and Lai, L., *J. Chem. Inf. Model*., 2007, vol. 47 p. 2140. https://doi.org/10.1021/ci700257y
41. Wildman, S.A. Crippen, G.M., *J. Chem. Inf. Comp. Sci*., 1999, vol. 39, p. 868. https://doi.org/10.1021/ci990307l
42. Lipinski, C.A., Lombardo, F., Dominy, B.W., and Feeney, P.J., *Adv. Drug. Deliv. Rev*., 2012, vol. 64, p. 4. https://doi.org/10.1016/j.addr.2012.09.019
43. Silicos-it. https://www.silicos-it.be
44. Daina, A., Michielin, O., and Zoete, V., *Sci. Rep.*, 2017, vol. 7, p. 1. https://doi.org/10.1038/srep42717
45. Delaney, J.S., *J. Chem. Inf. Comp. Sci*., 2004, vol. 44, p. 1000. https://doi.org/10.1021/ci034243x
46. Ali, J., Camilleri, P., Brown, M.B., Hutt, A.J., and Kirton, S.B., *J. Chem. Inf. Model*., 2012, vol 52, p. 2950. https://doi.org/10.1021/ci300447c
47. Ghose, A.K., Viswanadhan, V.N., and Wendoloski, J.J., *J. Comb. Chem*., 1999, vol. 1, p. 55. https://doi.org/10.1021/cc9800071
48. Veber, D.F., Johnson, S.R., Cheng, H.Y., Smith, B.R., Ward, K.W., and Kopple, K.D., *J. Med. Chem*., 2002, vol. 45, p. 2615. https://doi.org/10.1021/jm020017n
49. Egan, W.J., Merz, K.M., and Baldwin, J.J., *J. Med. Chem*., 2000, vol. 43, p. 3867. https://doi.org/10.1021/jm000292e

50. Muegge, I., Heald, S.L., and Brittelli, D., *J. Med. Chem*., 2001, vol. 44, p. 1841. https://doi.org/10.1021/jm015507e
51. Martin, Y.C., *J. Med. Chem*., 2005 vol. 48, p. 3164. https://doi.org/10.1021/jm0492002
52. Huber, K.P., and Herzberg, G., *Molecular Spectra and Molecular Structure IV*, New York: D. Van Nostrand Reinhold, Inc., 1979. https://doi.org/10.1007/978-1-4757-0961-2
53. Hill, T.L., *An Introduction to Statistical Thermodynamics*, London: Addison- Wesley Publishing, Inc., 1962. https://doi.org/10.1002/bbpc.19620660121
54. Serdaroğlu, G., *Int. J. Quantum Chem.*, 2010, vol. 111, p. 3938. https://doi.org/10.1002/qua.22809
55. Elik, M. and Serdaroğlu, G., *Cumhuriyet Sci. J.,* 2017, vol. 38, p. 138. https://doi.org/10.17776/csj.356185
56. Serdaroğlu, G., *Int. J. Quantum. Chem.*, 2011, vol. 111, p. 3938. https://doi.org/10.1002/qua.22809
57. Serdaroğlu, G., *Res. Chem. Intermediat.,* 2020, vol. 46, p. 961. https://doi.org/10.1007/s11164-019-04020-x